Journal of Materials Chemistry B

PAPER

View Article Online
View Journal | View Issue

Cite this: J. Mater. Chem. B, 2016, 4, 1448

Synthesis and characterization of porous carbon–MoS_2 nanohybrid materials: electrocatalytic performance towards selected biomolecules†

Joanna Dolinska,[a] Arunraj Chidambaram,[b] Witold Adamkiewicz,[a] Mehdi Estili,[c] Wojciech Lisowski,[a] Michalina Iwan,[a] Barbara Palys,[d] Ernst J. R. Sudholter,[b] Frank Marken,[e] Marcin Opallo*[a] and Liza Rassaei*[b]

Received 18th October 2015,
Accepted 25th January 2016

DOI: 10.1039/c5tb02175h

www.rsc.org/MaterialsB

Porous carbon nanohybrids are promising materials as high-performance electrodes for both sensing and energy conversion applications. This is mainly due to their high specific surface area and specific physicochemical properties. Here, new porous nanohybrid materials are developed based on exfoliated MoS_2 nanopetals and either negatively charged phenylsulfonated carbon nanoparticles or positively charged sulfonamide functionalized carbon nanoparticles. MoS_2 nanopetals not only act as a scaffold for carbon nanoparticles to form 3D porous hierarchical architectures but also result in well-separated electrochemical signals for different compounds. The characteristics of the new carbon nanohybrid materials are studied by dynamic light scattering, zeta potential analysis, high resolution X-ray photoelectron spectroscopy, transmission electron microscopy, scanning electron microscopy, infrared spectroscopy and electrochemistry. The new hybrid materials show superior charge transport capability and electrocatalytic activity toward selected biologically relevant compounds compared to earlier reports on porous carbon electrodes.

Introduction

Nanohybrid materials have been intensively studied for applications in catalysis over the last few decades due to their enhanced activity or synergistic effects compared to each single component. Here, we introduce a new type of porous nanohybrid materials consisting of charged carbon nanoparticles and two dimensional (2D) molybdenum disulphide. Porous carbons have been broadly used as high performance electrode materials in batteries,[1] fuel cells,[2,3] supercapacitors,[4] or sensors[5] mainly due to their high electrical conductivity, excellent thermal and chemical stability,[6] low density and broad availability. Among various carbon nanomaterials, carbon nanoparticles have been widely used in industry as fillers and pigments. Upon functionalization, these materials find even broader industrial applications and have been exploited as building blocks in thin film electrode systems[7–9] as their high level of reactive interfacial edge sites benefits electrochemical processes.[10] Current growing interest in design and synthesis of carbon nanohybrids with desired structures and specific physical/chemical properties stems from the need for more robust materials which benefit from the best of each component.[11–14]

Recently, graphene[15] and other two dimensional (2D) materials[16,17] have attracted much attention due to their unique physicochemical properties such as high conductivity and high surface energy. Another driving force for research on 2D materials comes from their potential use in sensing, (electro)catalysis, and energy applications. Next to graphene, 2D molybdenum disulphide has been mostly investigated due to its simple exfoliation process that originates from the weak van der Waals forces between the layers.[18,19] Numerous methods including wet exfoliation,[20,21] direct sulphurisation[22,23] and chemical vapour deposition[20,24] have been developed for exfoliation of MoS_2. Although each method has its own merit, ultimately they affect the properties and qualities of MoS_2 nanopetals. Exfoliated MoS_2 nanopetals consisting of few two dimensional layers exhibit semiconducting properties and their band gap energy increases by decreasing the number of layers.[25] The MoS_2 nanopetals exhibit electrocatalytic properties towards H_2 evolution,[19,26,27] and can be applied in microelectronics devices,[28–31] or for photocatalytic reactions.[32] Due to their well-developed surface,

[a] Institute of Physical Chemistry, Polish Academy of Sciences, ul. Kasprzaka 44/52, 01-224 Warszawa, Poland. E-mail: mopallo@ichf.edu.pl
[b] Organic Materials and Interfaces, Department of Chemical Engineering, Delft University of Technology, Delft, Netherlands. E-mail: l.rassaei@tudelft.nl
[c] Advanced Ceramics Group, Materials Processing Unit, National Institute for Materials Science (NIMS), Tsukuba 305-0047, Japan
[d] Faculty of Chemistry, University of Warsaw, Pasteura 1 Str., 02-093 Warsaw, Poland
[e] Department of Chemistry, University of Bath, Bath BA2 7AY, UK

† Electronic supplementary information (ESI) available. See DOI: 10.1039/c5tb02175h

MoS_2 nanopetals can be considered as an alternative for noble metal nanoparticles[19,26,28] (such as platinum nanoparticles in hydrogen evolution reactions),[33] or as a scaffold for other type of nanomaterials such as metallic nanoparticles[34,35] or carbon nanotubes[36] or reduced graphene oxide,[37,38] or as a base for *in situ* growth of metal nanoparticles.[39,40] Such strategy may result in nanohybrid materials with synergistic properties.[35] MoS_2 itself exhibits poor electrochemical properties, because of high resistance.[29,31] Therefore, its combination with metal nanoparticles or carbon nanomaterials is expected to facilitate its application as electrode materials for electrochemical processes.

Here, a new nanohybrid material of carbon nanoparticle-MoS_2 were introduced based on the decoration of MoS_2 nanopetals with negatively charged phenylsulfonated carbon nanoparticles or positively charged sulfonamide functionalized carbon nanoparticles. For this purpose, we selected negatively charged phenylsulfonated carbon nanoparticles (CNP−) commercially available from Emperor2000 and their positively charged counterparts (CNP+) where phenylsulfonated functionalities were converted to sulphonamides.[41] These nanoparticles belong to the wide range of functionalised carbon nanoparticles[42] and have previously exhibited electrocatalytic properties toward oxidation of biologically active compounds as ascorbic acid, dopamine and uric acid and separation of their electrochemical signals.[43,44] Interestingly, other MoS_2 hybrids with reduced graphene oxide and other components were recently prepared and applied for the same purpose.[37,38] The MoS_2 nanopetals decorated with carbon nanoparticles were characterised by XPS, TEM, SEM, IR spectroscopy, DLS, and zeta potential analysis. The superior electrocatalytic properties of these materials are demonstrated for selected biologically relevant compounds and compared with those of carbon nanoparticles.

Experimental

Materials

MoS_2, $K_3[Fe(CN)_6]$, ascorbic acid, dopamine, uric acid, epinephrine, and sodium dodecyl sulfate (SDS) were obtained from Sigma-Aldrich. HNO_3, HCl and H_2SO_4 were obtained from Chempur. All chemicals used in this work were of analytical grade. Ultrapure water (Millipore) was used for preparation of solutions. The negatively charged CNP were obtained from Cabot. Positively charged CNP were prepared by earlier described procedure.[41] Polishing pad and alumina slurries were obtained from Buehler.

Instrumentation

Surface characterization of all materials reported in this study such as MoS_2 precipitate and MoS_2 obtained from supernatant solution as well as porous carbon–MoS_2 nanohybrids was carried out by X-ray photoelectron spectroscopy (XPS), scanning electron microscopy (SEM) and EDX analysis. For these measurements, all samples were deposited on indium tin oxide glass substrate (ITO).

A PHI 5000 VersaProbe™ (ULVAC-PHI) spectrometer was used with monochromatic Al Ka radiation ($h\nu$ = 1486.6 eV) to survey and record high-resolution (HR) XPS spectra. X-ray beam was focused to a diameter of 100 μm and a defined measured area of 250 μm^2. The HR-XPS spectra were recorded with the hemispherical analyzer at the pass energy of 23.5 eV, the energy step size of 0.1 eV and the photoelectron take off angle 45° *versus* the surface plane. The XPS data were evaluated by the CasaXPS software. The binding energies of all spectra were calibrated with respect to the binding energies of C 1s at 284.6 eV.

The bright-field TEM images where taken using JEOL 2100F operating at 200 kV. For these experiments the hybrid materials were supported on a copper grid covered with a thin amorphous carbon film.

SEM and EDX analyses were performed with a Nova Nano-SEM 450 microscope with EDX detector from EDAX. Infrared spectra of samples deposited on ITO surface were recorded in reflectance mode using the Nicolet iN10-MX-FTIR microscope (Thermo Scientific) with the liquid nitrogen cooled MCT detector. An area of 100 μm^2 was sampled for a single spectrum. The spectral resolution was 4 cm^{-1} and typically 128 scans were averaged for a single spectrum. For the background collection, a bare ITO surface was used. Zeta potential and dynamic light scattering (DLS) measurements were performed using a Malvern ZetaSizer NanoZS instrument.

Cyclic voltammetry and chronoamperometry experiments were performed using a BioLogic SP-300 (Bio-Logic Science Instruments) electrochemical system with dedicated EC-Lab software v.10.19 in a conventional three electrode cell. Differential pulse voltammetry was performed with an Autolab, NoVa software 1.10 version. Glassy carbon disc electrode (0.007 cm^2, Minerals) was used as working electrode. For electrochemical measurements, platinum wire (d = 0.5 mm or d = 1 mm) and $Ag|AgCl|KCl_{sat.}$ were used as the counter and reference electrodes, respectively. All electrochemical experiments were carried out at 22 ± 2 °C.

Procedures

Preparation of MoS_2 nanopetals. MoS_2 nanopetals were prepared following earlier described procedure.[45] Typically, 0.1 g of MoS_2 and 0.1 mg SDS were added to 20 ml of demineralized water. This suspension was placed in an ultrasonic bath cleaner (VWR symphony) containing ice for 3.5 hours. This dispersion was further probe sonicated. After staying overnight and removing unexfoliated materials, the suspension was centrifuged. The final product was stored as a precipitate and a supernatant at 4 °C. Re-dispersed precipitate was used for further electrode modification.

Decoration of MoS_2 nanopetals. After re-dispersion in an ultrasonic bath, MoS_2 nanopetals suspension was mixed with earlier prepared CNP aqueous suspension (typically 0.1 g ml^{-1} for CNP− or 0.02 g ml^{-1} CNP+) in concentration ratio of 1 : 1. These samples were then ultrasonicated and centrifuged. The ready suspension of (MoS_2/CNP−), (MoS_2/CNP+) and (MoS_2/CNP+/CNP−) hybrids were used for solid substrate modification.

The size of both unmodified MoS_2 nanopetals and the ones decorated with carbon nanoparticles were estimated by DLS (Fig. S2, ESI†). The estimation was very crude and the size distribution was estimated as 300–500 nm for all samples. No clear effect of decoration was observed. Some aggregates were

evidently larger as they precipitate on the bottom of the test cuvette.

The zeta potential of MoS_2, MoS_2/CNP− and MoS_2/CNP+ suspensions was evaluated as −35, −41 and +27.7 mV indicating their high stability. The value obtained for MoS_2/CNP+/CNP− suspension was much lower: −16.7 mV indicating its low stability possibly due to the smaller repulsion between aggregates.

Electrode surface modification. For electrochemical measurements, glassy carbon electrodes were carefully polished on wet polishing pad with alumina slurry of 50 nm grain size. Next, the electrodes were rinsed with demineralized water, ethanol, and were placed in an ultrasonic bath. Finally, they were again rinsed with demineralized water, and dried with gentle argon/nitrogen flow. The glassy carbon electrodes were then modified *via* drop casting of 2 μl droplet of MoS_2 or decorated MoS_2 nanopetals suspension.

Results and discussion

Exfoliation and characterization of porous carbon–MoS_2 nanohybrids using XPS

MoS_2 was exfoliated following Coleman method[46] for sonication assisted liquid exfoliation of bulk MoS_2 powder. This exfoliation strategy relies on two steps, namely sonication and centrifugation. The sonication step deleteriously affects the van der Waals interaction between the layers of bulk MoS_2 to yield dimensionally reduced MoS_2 nanopetals, whereas the centrifugation step enables the separation of the nanosheet dispersion into thin layers. The supernatants and precipitates were then collected for further investigation. The use of SDS in exfoliation process changes the surface energy of the nanopetals and ensures that the MoS_2 nanopetals do not re-stack after exfoliation. The nanopetals produced here are comparatively thin mostly consisting of one or few MoS_2 layers.

High-resolution (HR) XPS was employed to study the chemical composition of MoS_2 precipitate and MoS_2 in supernatant samples. In analysis of HR-XPS spectra of MoS_2 precipitate and MoS_2 supernatant precipitate samples, we mainly focused on S 2p and Mo 3d signals (Fig. 1). The analysis of the S 2p spectra (Fig. 1A) reveals two states of sulfur at binding energies (BE) of the S $2p_{3/2}$ peak located at 161.5 eV and 168.5 eV, which can be assigned to sulfides and sulfates, respectively.[47] The sulfides appear to be the main sulfur state in the MoS_2 precipitate (originating from MoS_2) whereas sulfate were found to be a dominant sulfur state in the MoS_2 supernatant (originating from the presence of SDS). The analysis of the de-convoluted Mo 3d spectra (Fig. 1B) discloses three Mo states (at binding energies of the Mo $3d_{5/2}$ peak at 228.4 eV, 230.8 eV and 232.2 eV), which can be ascribed to MoS_2 (MoO_2), MoO_4^{2-} and MoO_3, respectively.[44] The MoS_2 was detected as main Mo state in the MoS_2 precipitate, whereas the relative contribution of MoO_4^{2-} and MoO_3 compounds becomes more significant in the MoS_2 supernatant.

MoS_2 nanopetals were then decorated with positively charged sulfonamide functionalized carbon nanoparticles and/or negatively charged sulfonyl functionalized carbon nanoparticles. HR-XPS analysis was performed to explore the effect of carbon nanoparticle charge on the chemical states of MoS_2 nanopetals. In Fig. 2, the HR-XPS spectra of S 2p, N 1s, Mo 3d and C 1s of (MoS_2/CNP−), (MoS_2/CNP+) and (MoS_2/CNP+/CNP−) are presented and compared.

The S 2p HR spectra of decorated MoS_2 nanopetals (Fig. 2A) reveal two states of sulfur (the S $2p_{3/2}$ peak placed at binding

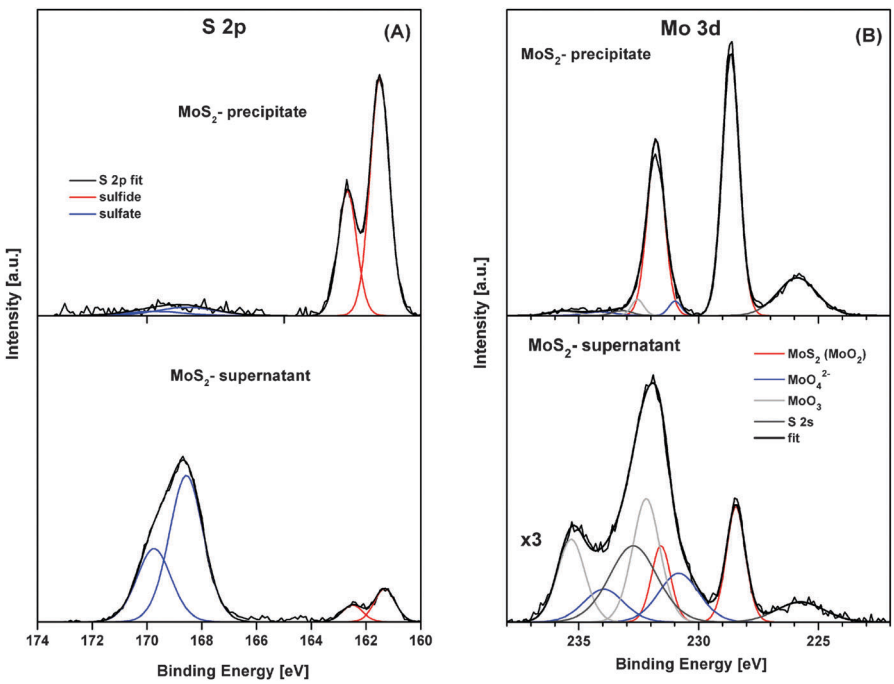

Fig. 1 High-resolution XPS spectra of S 2p (A) and Mo 3d (B) of MoS_2 precipitate and MoS_2 supernatant. De-convoluted peaks identify various chemical compounds of sulfur and molybdenum.

energies of 162.3–162.5 eV and 168.3–168.9 eV), which can be assigned to sulfides and sulfones (sulfates), respectively.[47] The relative contribution ratio of the sulfones (sulfates) to sulfide compounds was roughly estimated to be 0.6, 2.2 and 4.9 for (MoS_2/CNP+), (MoS_2/CNP−) and (MoS_2/CNP+/CNP−) samples, respectively. The analysis of the N 1s spectra (Fig. 2B) is complicated by overlapping with the Mo $2p_{3/2}$ XPS peak.[47] However, only few specific XPS data are available for surface bound sulfonamide compounds.[41,48] A pair of N 1s peaks at binding energies of 394.7 eV and 400.8 eV have been previously reported by Watkins *et al.*[41] Similar pairs of XPS peaks, referred to un-protonated and protonated amine, have also been reported for ammonia adsorbed on graphite oxides.[49] Assuming the N 1s peak separation of 6.1 eV[41] and taking the well-controlled position of the overlapping Mo $2p_{3/2}$ peak,[44] N 1s spectra of (MoS_2/CNP+) and (MoS_2/CNP+/CNP−) samples were convoluted (Fig. 2B). The N 1s peaks at binding energies of 394.3 eV and 400.4 eV are consistent with the N 1s signals reported previously.[41] From the

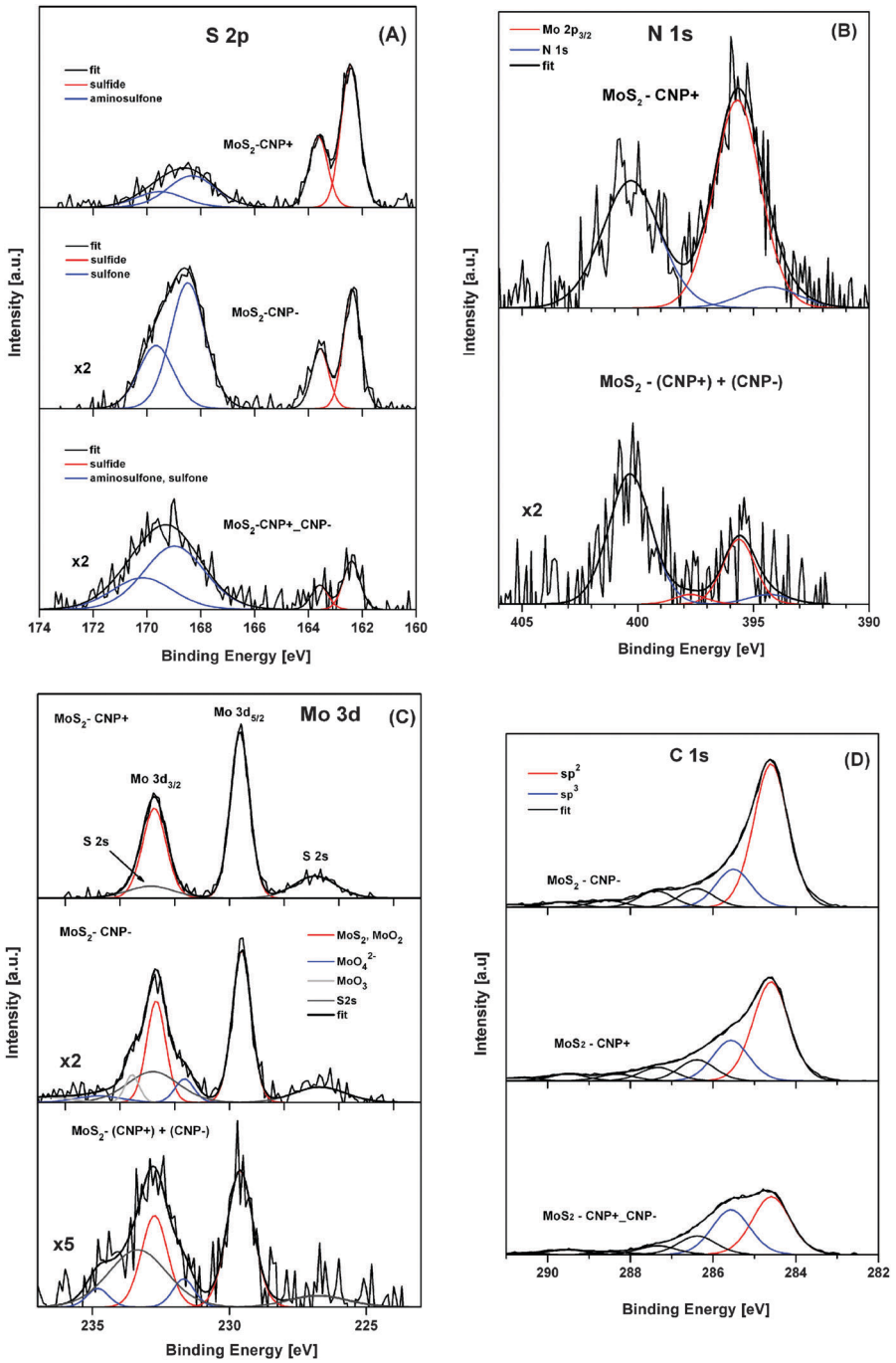

Fig. 2 High-resolution XPS spectra of S 2p (A), N 1s (B), Mo 3d (C) and C 1s (D) monitored for (MoS_2/CNP−), (MoS_2/CNP+) and (MoS_2/CNP+/CNP−) samples. De-convoluted peaks present various chemical compounds of sulphur, nitrogen, molybdenum and carbon, respectively.

nitrogen N 1s peaks and sulfur S 2p peaks a relative atomic concentration ratio of 0.7 and 0.4 were estimated for (MoS_2/CNP+) and (MoS_2/CNP+/CNP−), respectively, indicating larger coverage of MoS_2 by CNP+.

Fig. 2C shows the complex Mo 3d spectra, partially overlapped by S 2s peaks, which were obtained for MoS_2/CNP samples. The Mo $3d_{5/2}$ peak at a binding energy of 229.6 eV, identified as MoS_2 (MoO_2) compound, was found to be a dominant Mo state in all samples. However, for the (MoS_2/CNP−) and (MoS_2/CNP+/CNP−) samples, a relative increase of Mo 3d peaks was observed at a binding energy higher than 231 eV, which can be assigned to MoO_4^{2-} and MoO_3.

The C 1s spectra, recorded for all MoS_2/CNP samples (Fig. 2D), reveals a different contents of sp^2 and sp^3 hybridized carbon atoms. Deconvoluted spectra reveal characteristic carbon states that are represented by the C 1s peaks at binding energies of 284.6 eV and 285.5 eV, respectively.[50] The sp^2/sp^3 atomic concentration ratios for (MoS_2/CNP−), (MoS_2/CNP+) and (MoS_2/CNP+/CNP−) samples, were estimated to be 3.8, 2.4 and 1.3, respectively. These values indicate different carbon bond character in the MoS_2/CNP nanostructures which are stabilized by negatively and positively charged functional groups.

The carbon coverage of MoS_2 nanopetals evaluated for (MoS_2/CNP−), (MoS_2/CNP+) and (MoS_2/CNP+/CNP−) samples decreases in a sequence of 1 : 0.9 : 0.7, which is in line with sp^2/sp^3 change tendency. Meanwhile, oxygen contents increases as 1 : 1.3 : 2.1, respectively. The O/(C + S + Mo + N) atomic concentration ratios for (MoS_2/CNP−), (MoS_2/CNP+) and (MoS_2/CNP+/CNP−) samples, were estimated to be 0.22, 0.34 and 0.65, respectively. Thus, it is likely that the formation of oxidized states of elemental surface species (Fig. S3, ESI†) influences the sp^2/sp^3 carbon bound character in MoS_2/CNP samples.

Comparison with XPS spectra of non-decorated MoS_2 samples (Fig. 1) clearly indicates that the MoS_2 nanopetals are decorated with carbon nanoparticles and their specific features agree well with the chemical nature of nanoparticles functional groups.

TEM imaging of porous carbon–MoS_2 nanohybrids

Fig. 3 shows typical bright-field transmission electron microscopy (TEM) images of rather large MoS_2 nanopetals, which are uniformly covered by fine amorphous CNP nanoparticles (A–D). These hybrid nanopetals are building blocks of the samples shown in Fig. 4 (SEM images). It is evident that such 2D nanobuilding blocks when assembled together would create 3D porous microstructures with large useable/active surface area. The porosity is formed due to existence of the CNP nanoparticles between the MoS_2 nanopetals preventing their restacking as well as the existence of space between the distributed CNPs and natural pores within the CNP agglomerates as clearly shown in Fig. 3D. The individual CNPs aggregates (having irregular shapes) seem to have amorphous structure according to Fig. 3E.

SEM images of porous carbon–MoS_2 nanohybrids

SEM images of the samples prepared by drop casting of MoS_2 nanopetals (both precipitates and supernatants) show their random aggregates distributed on ITO surface (Fig. 4A, Fig. S4 and S5, ESI†) with a size distribution in agreement with that obtained from DLS measurements (300–500 nm diameter). Close inspection of MoS_2 stacks on ITO surface suggests that the exfoliation is not entirely effective or MoS_2 nanopetals re-stack upon drying (Fig. 4A). Single broken nanopetals are observed on the aggregate surface obtained from exfoliation using sonic probe. This well-developed structure was selected for further modification with carbon nanoparticles. On the other hand, more single nanopetal structures are observed for MoS_2 supernatant solution (Fig. S3, ESI†).

Addition of positively or negatively charged carbon nanoparticles results in a porous carbon–MoS_2 nanohybrides where MoS_2 nanopetal surfaces are entirely covered with carbon nanoparticles. Fig. 4B–D show SEM images of the samples prepared from (MoS_2/CNP−) or (MoS_2/CNP+) suspension indicating that the surfaces and edges are covered by aggregates of the size of 20–40 nm which can be identified as carbon nanoparticles. No clear effect of the carbon nanoparticle's charge on the structure is observed indicating that MoS_2 nanopetals can be decorated with both types of nanoparticles. This occurs despite the fact that the MoS_2 surface is partially negatively charged.[20,51,52] Also SEM images of the deposit prepared from (MoS_2/CNP−/CNP+) show the coverage of MoS_2 aggregates by nanoparticles (Fig. 4D). Clearly in all cases, the MoS_2 materials with a well-developed surface are covered by carbon nanoparticles.

Interestingly carbon nanoparticles entirely cover the MoS_2 nanopetals surfaces regardless of their charge. Once drop casted, the MoS_2 layers on the electrode are stable during the measurements, or even after sonication of *ca.* 30 s.

IR spectroscopy of porous carbon–MoS_2 nanohybrids

Next, (MoS_2/CNP+), (MoS_2/CNP−) and (MoS_2/CNP−/CNP+) films were studied by IR spectroscopy (Fig. 5). The spectrum of (MoS_2/CNP+) reveals a wide band at 1139 cm^{-1} corresponding to mixed contributions from the SO_2 group as well as to CH bending motions of the phenyl ring. The intense doublet at 1584 and 1678 cm^{-1} corresponds to the NH deformation modes of the protonated amine groups.[53] The NH stretching motions rise to the very wide band from 3000 to 3600 cm^{-1}. The intense and relatively wide bands of the amine groups as well as SO_2 group suggest the formation of hydrogen bonds between amine and SO_2 groups. Such hydrogen bonds could be formed among sulfonamide groups of the neighboring particles, contributing to the easy decoration of MoS_2 by CNP+. The spectrum of (MoS_2/CNP+) reveal quite intense bands at 2850 and 2919 cm^{-1} signifying the presence of CH_2 groups. The most intense multiple bands in the (MoS_2/CNP−) spectra from 1000 to 1300 cm^{-1}, correspond to the asymmetric and symmetric S–O stretching motions of the SO_3^- group.[53] Further band splitting might be caused by coupling between neighboring SO_3^- groups. The band at 1595 cm^{-1} corresponds to phonon modes of carbon nanoparticles.[54] In the case of (MoS_2/CNP+), this band overlaps with the strong bands of protonated amines.

The band at 1720 cm^{-1} signifies the presence of carbonyl moieties on CNP surface, which are not removed during the

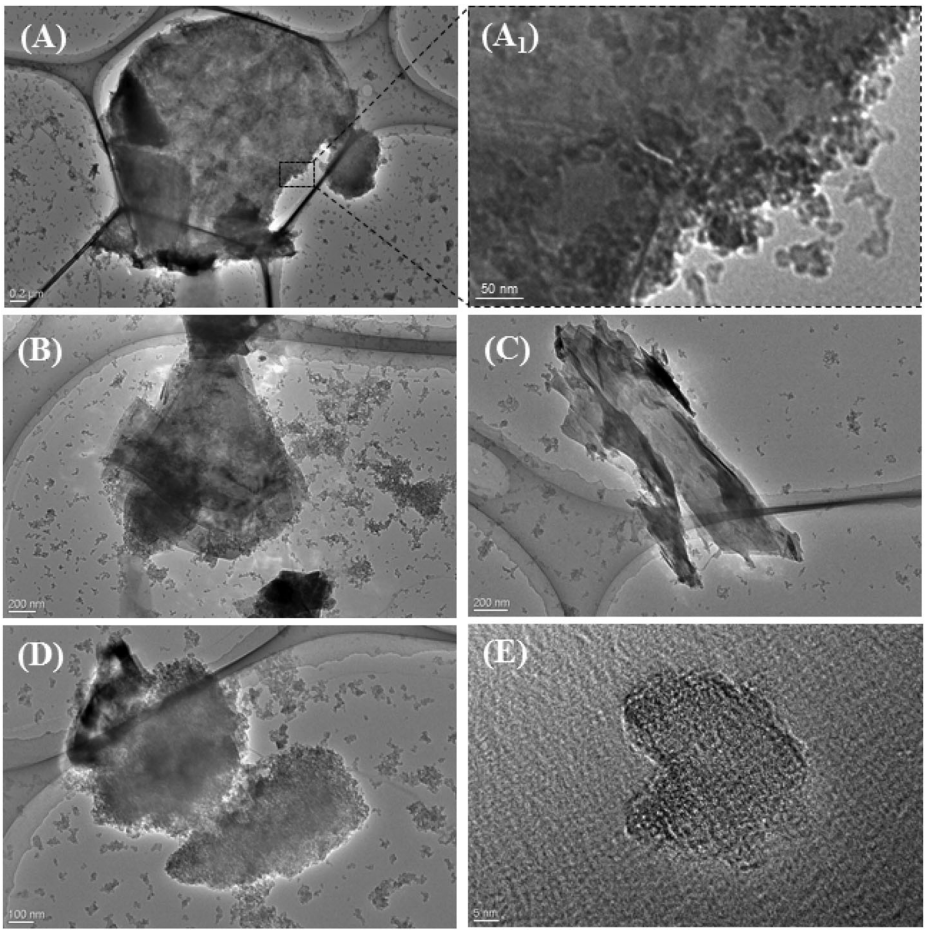

Fig. 3 Bright-field transmission electron microscopy (TEM) images of CNP-covered MoS_2 nanopetals: (A) a large MoS_2 nanopetal uniformly covered with fine CNP nanoparticles; (A_1) enlarged view of the selected region clearly showing the individual CNP nanoparticles on MoS_2 surface. (B–D) Other typical examples of the CNP-covered MoS_2 nanopetals. (E) A typical high-resolution image of individual CNP nanoparticles.

modification procedure. The wide band centered about 3000 cm^{-1} originates probably from C–H surface groups.

IR spectrum of (MoS_2/CNP−/CNP+) includes signatures from both sulfonamide and sulfonic groups, though the relative intensities of the band are altered. The N–H stretching mode (3290 cm^{-1}) is less intense and narrower. The components of the doublet due to the NH_3^+ deformation modes shift from 1584 and 1678 cm^{-1} (MoS_2/CNP+) to 1600 and 1665 cm^{-1} (MoS_2/CNP−/CNP+). All components of the SO_3^- multiple band in the (MoS_2/CNP−) spectrum are reproduced in the MoS_2/CNP−/CNP+ spectrum, though the relative intensities are altered. This change is possibly due to the charge distribution, resulting from electrostatic interaction between SO_3^- and NH_3^+ groups.

Electrocatalytic performance

Electrochemical properties of the studied nanohybrids were examined on glassy carbon electrodes by cyclic voltammetry in a solution of 1 mM $Fe(CN)_6^{3-}$ redox probe. As shown in Fig. 6A, the modification of glassy carbon electrodes with just MoS_2 does not significantly affect the voltammetric signal, whereas upon modification with (MoS_2/CNP−), (MoS_2/CNP+) or (MoS_2/CNP−/CNP+), both the magnitude of capacitive currents and the peak currents significantly increases. This is mainly due to the increase in electrochemically active surface area in presence of CNPs confirmed by chronoamperometry experiments (Fig. S6, ESI†). Carbon nanoparticles cover the MoS_2 nanopetals such that electrical contact between them (percolation paths) and with the glassy carbon surface is preserved. The estimated surface area ratios are 1 : 0.8 : 11.4 : 4.2 for bare glassy carbon electrode and the one modified with MoS_2, (MoS_2/CNP+), and (MoS_2/CNP−), respectively. This indicates larger coverage of MoS_2 nanopetals with CNP+ due to electrostatic attractions between negatively charged nanopetals and positively charged sulfonamide functionalities on carbon nanoparticles. The reduced voltammetric peaks separation of 0.15 V corresponding to redox process of $Fe(CN)_6^{3-/4-}$ at carbon nanoparticle modified electrodes indicate a more reversible process compare to that at glassy carbon electrode. The voltammograms are stable during subsequent cycles indicating stability of the modified electrodes. The robustness of the modified electrodes is especially noteworthy as they can endure at least 30 s sonication.

Electrocatalytic properties of these nanohybrid materials were next examined for biologically relevant compounds. Epinephrine also known as adrenaline is both an important hormone and

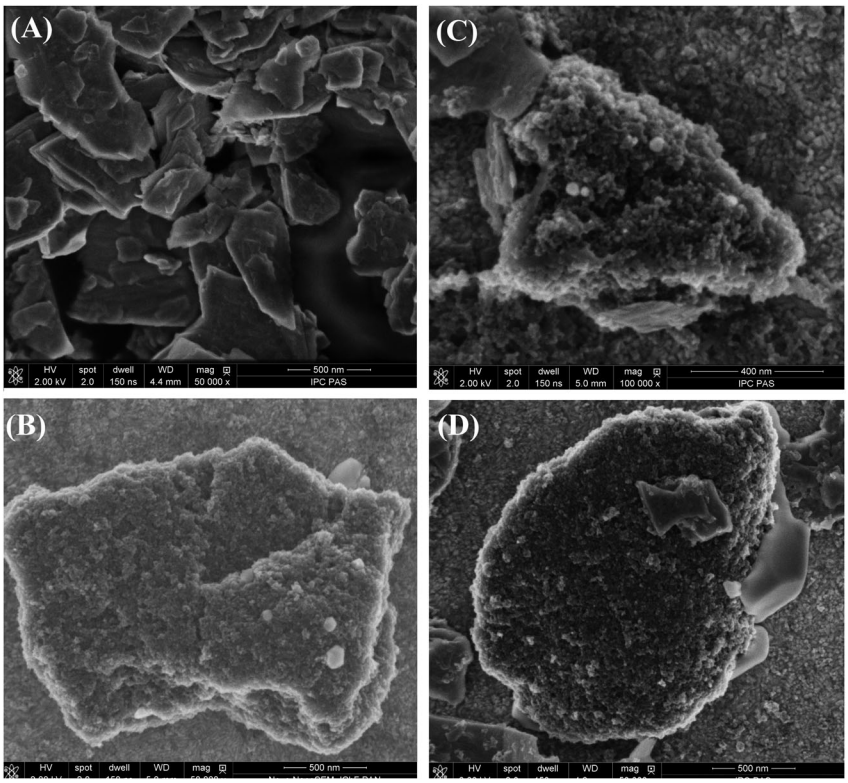

Fig. 4 SEM images of the precipitates obtained from (A) exfoliated MoS_2 precipitate, (B) (MoS_2/CNP−), (C) (MoS_2/CNP+) and (D) (MoS_2/CNP+/CNP−) suspensions on an ITO surface.

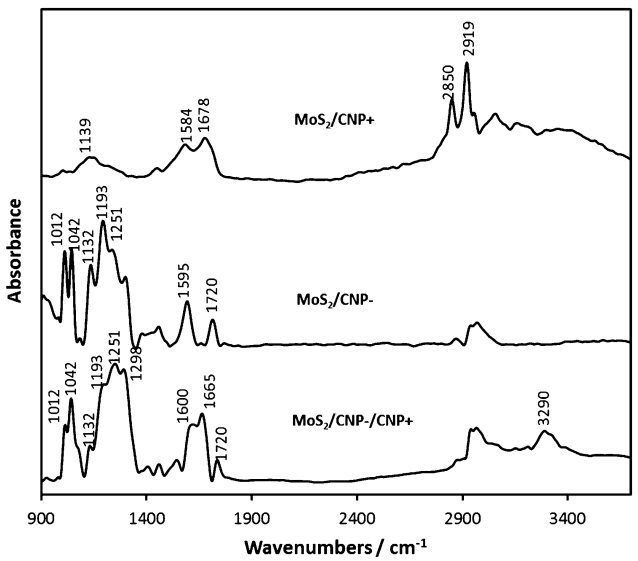

Fig. 5 Infrared spectra of (MoS_2/CNP+), (MoS_2/CNP−) and (MoS_2/CNP−/CNP+).

neurotransmitter and also used as a drug for treatment of disease such as hypertension. Thus, its sensitive measurement is important in medicine and requires robust advanced materials that can be integrated in sensing platforms. Cyclic voltammograms in Fig. 6B clearly demonstrate electrocatalytic activity of the modified electrodes for the oxidation of epinephrine. The onset potential of epinephrine oxidation at glassy carbon electrode (0.34 V *vs.* Ag|AgCl) shifts to lower potentials (0.17 V *vs.* Ag|AgCl) once it is modified with MoS_2–carbon nanoparticles nanohybrids indicating electrocatalytic activity of the modified electrodes. Although this shift is almost similar for all modified electrodes, MoS_2/CNP− film shows superior electrocatalytic properties in terms of current density. On the basis of the amount of carbon nanoparticles estimated from XPS data (see below) one would expect largest current density for (MoS_2/CNP+) film. Perhaps other factors as their aggregation, the electric charge of their functionalities and the electrostatic interaction with the scaffold and with the substrate may play important role.

The electrocatalytic activity of the nanohybrids modified electrodes was also investigated for dopamine. Dopamine (DA) is a neurotransmitter that regulates our movement and emotional responses.[55] A major problem with measurement of dopamine stems from the low resolution between DA and interferences such as ascorbic acid and uric acid. Thus, improvement of the electrode selectivity for measurement of dopamine over interfering species has been the focus of many research.[56–58] Fig. 6C shows the cyclic voltammograms of 2 mM dopamine in presence of ascorbic acid and uric acid. For bare glassy carbon electrode, only one oxidation peak at 0.49 V *vs.* Ag|AgCl with a shoulder at 0.34 V *vs.* Ag|AgCl was observed. For (MoS_2/CNP+) modified glassy carbon electrode, one not well-formed oxidation peak at 0.13 V, and two clear oxidation peaks at 0.42 V, and 0.54 V *vs.* Ag|AgCl were observed corresponding to the ascorbic acid, dopamine, and uric acid. The location of the oxidation peaks are almost similar to that

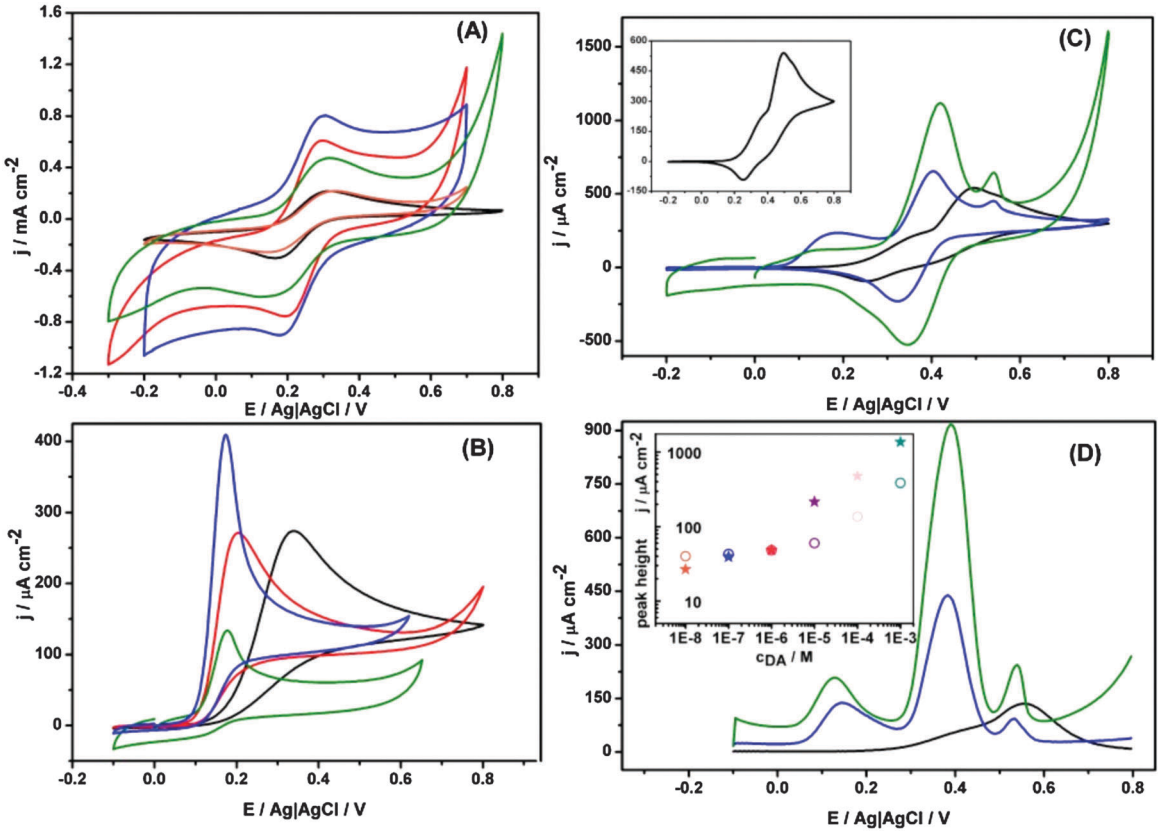

Fig. 6 (A) Cyclic voltammograms (scan rate 0.01 V s^{-1}) obtained in 1 mM $K_3[Fe(CN)_6]$ solution in 0.1 M phosphate buffer solution (pH 7.4) on bare glassy carbon electrode (black) and modified with MoS_2 (orange), (MoS_2/CNP−) (blue), (MoS_2/CNP+) (green), and (MoS_2/CNP−/CNP+) (red), (B) cyclic voltammograms (scan rate 0.1 V s^{-1}) obtained for bare glassy carbon electrode (black) and modified with (MoS_2/CNP−) (blue), (MoS_2/CNP+) (green), and (MoS_2/CNP−/CNP+) (red) in 1 mM epinephrine in 0.1 M phosphate buffer solution (pH 7.4), (C) cyclic voltammograms (scan rate 0.1 V s^{-1}) and (D) differential pulse voltammograms obtained in 2 mM dopamine (DA) 1 mM ascorbic acid (AA) and 1 mM uric acid (UA) in the in 0.1 M phosphate buffer solution (pH 4.8). The experiments were performed with bare GC electrode (black) and modified with (MoS_2/CNP−) (blue), (MoS_2/CNP+) (green). The inset in (C) shows the cyclic voltammograms of a bare glassy carbon electrode. The inset in (D) shows the concentration dependence (1×10^{-8}–1×10^{-3} M) peak current at 0.4 V in the 1 mM ascorbic acid (AA) and 1 mM uric acid (UA) in the in 0.1 M phosphate buffer solution (pH 4.8).

observed for either of positively and negatively charged nanoparticles modified glassy carbon electrode (Fig. S7–S9, ESI†) with clear distinction that the current density has massively increased. Interestingly, only one reduction peak is observed and can be attributed to the reduction of dopamine as the oxidation of ascorbate and urate under these conditions are irreversible. Once the electrode is modified with MoS_2/CNP−, three well-defined oxidation peaks at 0.18, 0.40, and 0.54 V *vs.* Ag|AgCl were observed indicating superior properties of the nanohybrid materials for selective detection of the above compounds. The superior electrocatalytic properties of MoS_2/CNP− can be related to the negative surface charge of the hybrid materials and repulsion of ascorbate and urate from their surface. These results are in agreement with those obtained from differential pulse voltammetry as presented in Fig. 6D. Although the concentration dependence is not linear in the whole concentration range studied the limit of detection reaches 1×10^{-8} M.

Fig. S7–S9 (ESI†) also demonstrate that the presence of MoS_2 increases the voltammetric currents as compared to electrodes modified only with CNP. Thus, MoS_2 nanopetals have dual contributions: current enhancement due to larger electroactive surface and better peak separation – the onset potential for electro-oxidation of ascorbic acid and dopamine shifts to lower potentials. MoS_2 nanopetals as scaffolds for carbon nanoparticles (in agreement with SEM images, Fig. 3), play an important role in electrodes stability and charge transfer properties. Table S1 (ESI†) presents a comparison of the results obtained for dopamine in this study with those of reported literature using various carbon materials without MoS_2 nanopetals. Superior catalytic properties of MoS_2/CNP nanohybrids are evident from this table.

Conclusion

A facile approach was successfully developed for the rapid preparation of porous carbon–MoS_2 nanohybrids based on negatively or positively charged carbon nanoparticles and MoS_2 nanopetals. The MoS_2 nanopetals mainly act as a scaffold for carbon nanoparticles providing 3D porous hierarchical architectures regardless of their charge. The superior charge transport property of these new nanohybrid materials were demonstrated by their enhanced

electrocatalytic activity towards oxidation of several biologically relevant compounds. More research is required to investigate the effect of carbon nanoparticles size, the ratio of positively and negatively charged carbon nanoparticles, the number and size of MoS_2 nanosheets, and the surfactant charge during exfoliation process on final nanohybrid structure. Potential application of these hybrid materials in other platforms such as sensors, lithium batteries, or supercapacitors worth extensive studies.

Acknowledgements

This work was partially sponsored by the National Science Centre (Project No. 2011/03/B/ST4/02620). Purchase of Scanning Electron Microscope from resources of NanOtechnology, Biomaterials and aLternative Energy Source for ERA integration grant (FP7-REGPOT-CT-2011-285949-NOBLESSE) is gratefully acknowledged. Supply of carbon nanoparticles from Cabot Corporation is gratefully acknowledged. A. C. and J. D. gratefully thank Dr Zahra Taleat for helpful discussions. J. D. also thank Dr Ievgen Obraztsov for helpful discussions.

References

1 Q. Zhang, X. Cheng, J. Huang, H. Peng and F. Wei, *Carbon*, 2015, **81**, 850.
2 G. Liu, Y. Zhang, J. Cai, X. Zhang and J. Qiu, *Carbon*, 2015, **86**, 371.
3 P. Trogadas, T. F. Fuller and P. Strasser, *Carbon*, 2014, **75**, 5–42.
4 H. Chen, S. Zeng, M. Chen, Y. Zhang and Q. Li, *Carbon*, 2015, **92**, 271–296.
5 K. Ariga, Y. Yamauchi, Q. Ji, Y. Yonamine and J. P. Hill, *APL Mater.*, 2014, **2**, 030701.
6 M.-M. Titirici, R. J. White, N. Brun, V. L. Budarin, D. S. Su, F. del Monte, J. H. Clark and M. J. MacLachlan, *Chem. Soc. Rev.*, 2015, **44**, 250–290.
7 L. Rassaei, M. Sillanpää and F. Marken, *Electrochim. Acta*, 2008, **53**, 5732–5738.
8 N. Cheng, R. A. Webster, M. Pan, S. Mu, L. Rassaei, S. C. Tsang and F. Marken, *Electrochim. Acta*, 2010, **55**, 6601–6610.
9 L. Rassaei, M. Sillanpää, K. J. Edler and F. Marken, *Electroanalysis*, 2009, **21**, 261–266.
10 R. L. McCreery, *Chem. Rev.*, 2008, **108**, 2646–2687.
11 G. Wang, X. He, L. Wang, A. Gu, Y. Huang, B. Fang, B. Geng and X. Zhang, *Microchim. Acta*, 2013, **180**, 161–186.
12 S. H. Joo, S. J. Choi, I. Oh, J. Kwak, Z. Liu, O. Terasaki and R. Ryoo, *Nature*, 2001, **412**, 169–172.
13 M. Oyama, *Anal. Sci.*, 2010, **26**, 1–12.
14 B. Wu, Y. Kuang, X. Zhang and J. Chen, *Nano Today*, 2011, **6**, 75–90.
15 X. Li, Y. Zhu, W. Cai, M. Borysiak, B. Han, D. Chen, R. D. Piner, L. Colomba and R. S. Ruoff, *Nano Lett.*, 2009, **9**, 4359–4363.
16 M. Pumera and A. H. Loo, *TrAC, Trends Anal. Chem.*, 2014, **61**, 49–53.
17 F. Pu, High Yield Production of Inorganic Graphene-Like Testing Key Parameters Fei Pu High Yield Production of Inorganic Graphene-Like Materials (MoS_2, WS_2, BN) Through Liquid Exfoliation Testing Key Parameters, Bachelor thesis, 2012, pp. 1–41.
18 F. S. Freitas, A. S. Gonçalves, A. De Morais, J. E. Benedetti and F. Ana, *NanoGe J. Ener. Sust.*, 2013, 1–5.
19 S. Ji, Z. Yang, C. Zhang, Z. Liu, W. W. Tjiu, I. Y. Phang, Z. Zhang, J. Pan and T. Liu, *Electrochim. Acta*, 2013, **109**, 269–275.
20 M. Chhowalla, H. S. Shin, G. Eda, L.-J. Li, K. P. Loh and H. Zhang, *Nat. Chem.*, 2013, **5**, 263–275.
21 A. Winchester, S. Ghosh, S. Feng, A. L. Elias, T. Mallouk, M. Terrones and S. Talapatra, *ACS Appl. Mater. Interfaces*, 2014, **6**, 2125–2130.
22 D. Kong, H. Wang, J. J. Cha, M. Pasta, K. J. Koski, J. Yao and Y. Cui, *Nano Lett.*, 2013, **13**, 1341–1347.
23 A. P. S. Gaur, S. Sahoo, M. Ahmadi, M. J. F. Guinel, S. K. Gupta, R. Pandey, S. K. Dey and R. S. Katiyar, *J. Phys. Chem. C*, 2013, **117**, 26262–26268.
24 O. Lopez-Sanchez, D. Lembke, M. Kayci, A. Radenovic and A. Kis, *Nat. Nanotechnol.*, 2013, **8**, 497–501.
25 K. F. Mak, C. Lee, J. Hone, J. Shan and T. F. Heinz, *Phys. Rev. Lett.*, 2010, **105**, 2–5.
26 X. Bian, J. Zhu, L. Liao, M. D. Scanlon, P. Ge, C. Ji, H. H. Girault and B. Liu, *Electrochem. Commun.*, 2012, **22**, 128–132.
27 X. Xia, Z. Zheng, Y. Zhang, X. Zhao and C. Wang, *Int. J. Hydrogen Energy*, 2014, **39**, 9638–9650.
28 H. Wang, Z. Lu, S. Xu, D. Kong, J. J. Cha, G. Zheng, P.-C. Hsu, K. Yan, D. Bradshaw, F. B. Prinz and Y. Cui, *Proc. Natl. Acad. Sci. U. S. A.*, 2013, **110**, 19701–19706.
29 G. a. Salvatore, N. Münzenrieder, C. Barraud, L. Petti, C. Zysset, L. Büthe, K. Ensslin and G. Tröster, *ACS Nano*, 2013, **7**, 8809–8815.
30 B. Radisavljevic, A. Radenovic, J. Brivio, V. Giacometti and A. Kis, *Nat. Nanotechnol.*, 2011, **6**, 147–150.
31 R. Ganatra and Q. Zhang, *ACS Nano*, 2014, **8**, 4074–4099.
32 Z. Yin, B. Chen, M. Bosman, X. Cao, J. Chen, B. Zheng and H. Zhang, *Small*, 2014, 3537–3543.
33 W. Sheng, H. A. Gasteiger and Y. Shao-Horn, *J. Electrochem. Soc.*, 2011, **157**, B1398–B1404.
34 H. S. S. R. Matte, U. Maitra, P. Kumar, B. Govinda Rao, K. Pramoda and C. N. R. Rao, *Z. Anorg. Allg. Chem.*, 2012, **638**, 2617–2624.
35 J. Dolinska, A. Chidambaram, Z. Taleat, W. Adamkiewicz, W. Lisowski, B. Palys, M. Holdynski, T. Andryszewski, V. Sashuk, L. Rassaei and M. Opallo, *Electrochim. Acta*, 2015, **182**, 659–667.
36 V. O. Koroteev, A. V. Okotrub, Y. V. Mironov, O. G. Abrosimov, Y. V. Shubin and L. G. Bulusheva, *Inorg. Mater.*, 2007, **43**, 236–239.
37 K. Pramoda, K. Moses, U. Maitra and C. N. R. Rao, *Electroanalysis*, 2015, **27**, 1892–1898.
38 L. Xing and Z. Ma, *Microchim. Acta*, 2016, **183**, 257–263.
39 Y. Shi, J.-K. Huang, L. Jin, Y.-T. Hsu, S. F. Yu, L.-J. Li and H. Y. Yang, *Sci. Rep.*, 2013, **3**, 1839.

40 S. Su, H. Sun, F. Xu, L. Yuwen and L. Wang, *Electroanalysis*, 2013, **25**, 2523–2529.
41 J. D. Watkins, R. Lawrence, J. E. Taylor, S. D. Bull, G. W. Nelson, J. S. Foord, D. Wolverson, L. Rassaei, N. D. M. Evans, S. A. Gascon and F. Marken, *Phys. Chem. Chem. Phys.*, 2010, **12**, 4872–4878.
42 K. Lawrence, C. L. Baker, T. D. James, S. D. Bull, R. Lawrence, J. M. Mitchels, M. Opallo, O. a. Arotiba, K. I. Ozoemena and F. Marken, *Chem. – Asian J.*, 2014, **9**, 1226–1241.
43 A. Celebanska, D. Tomaszewska, A. Lesniewski and M. Opallo, *Biosens. Bioelectron.*, 2011, **26**, 4417–4422.
44 E. Rozniecka, M. Jonsson-Niedziolka, A. Celebanska, J. Niedziolka-Jonsson and M. Opallo, *Analyst*, 2014, **139**, 2896–2903.
45 D. Gopalakrishnan, D. Damien and M. M. Shaijumon, *ACS Nano*, 2014, **8**, 5297–5303.
46 R. J. Smith, P. J. King, M. Lotya, C. Wirtz, U. Khan, S. De, A. O'Neill, G. S. Duesberg, J. C. Grunlan, G. Moriarty, J. Chen, J. Wang, A. I. Minett, V. Nicolosi and J. N. Coleman, *Adv. Mater.*, 2011, **23**, 3944–3948.
47 A. M. Venezia, *Catal. Today*, 2003, **77**, 359–370.
48 G. A. Schick and Z. Q. Sun, *Langmuir*, 1994, **10**, 3105–3110.
49 C. Petit, M. Seredych and T. J. Bandosz, *J. Mater. Chem.*, 2009, **19**, 9176.
50 P. Mérel, M. Tabbal, M. Chaker, S. Moisa and J. Margot, *Appl. Surf. Sci.*, 1998, **136**, 105–110.
51 J. Heising and M. G. Kanatzidis, *J. Am. Chem. Soc.*, 1999, **121**, 11720–11732.
52 L. Messio, C. Lhuillier and G. Misguich, *Phys. Rev. B: Condens. Matter Mater. Phys.*, 2013, **87**, 125127.
53 G. Socrates, *Infrared and Raman characteristic group frequencies*, 2004.
54 U. Kuhlmann, H. Jantoljak, N. Pfänder, P. Bernier, C. Journet and C. Thomsen, *Chem. Phys. Lett.*, 1998, **294**, 237–240.
55 J.-M. Beaulieu and R. R. Gainetdinov, *Pharmacol. Rev.*, 2011, **63**, 182–217.
56 K. Jackowska and P. Krysinski, *Anal. Bioanal. Chem.*, 2013, **405**, 3753–3771.
57 C. R. Raj, T. Okajima and T. Ohsaka, *J. Electroanal. Chem.*, 2003, **543**, 127–133.
58 I. S. Muratova, L. A. Kartsova and K. N. Mikhelson, *Sens. Actuators, B*, 2014, **207**, 900–906.